Journal of Sound and Vibration (1999) **219**(5), 881–904
Article No. jsvi.1998.1939, available online at http://www.idealibrary.com on IDEAL

THE EFFECTS OF LOCAL PRELOAD ON THE FOUNDATION STIFFNESS AND VERTICAL VIBRATION OF RAILWAY TRACK

T. X. Wu† and D. J. Thompson

*Institute of Sound and Vibration Research, University of Southampton, Highfield, Southampton SO*17 1*BJ, England*

(*Received* 19 *June* 1998, *and in final form* 27 *August* 1998)

Track vibration is one of the main sources of railway rolling noise. The resilient components in the railway foundation such as the pad and ballast have significant effects on the track vibration. Usually, their parameters vary with load and frequency. The wheel load of a train causes local deformation in the track and the foundation, so the railpads and the ballast are preloaded and thus their stiffness has different values at the supports near the wheel load from the other supports. In this paper the preloads in the pad and ballast caused by a single wheel load are studied by considering the non-linear properties of the track foundation, and thus the preloaded pad and ballast stiffnesses are determined. A model of the track dynamics based on an infinite discretely supported Timoshenko beam with preloaded pad and ballast dynamic stiffnesses is developed. Its vertical vibration behaviour under the influence of the local wheel load is investigated. It is shown that the point receptance for vertical vibration is strongly affected by the local wheel load at low frequencies, but the effect of the local wheel load on the average wave propagation decay rate along the rail is very limited.

1. INTRODUCTION

Railway rolling noise is an important environmental issue which forms the principal source of noise from railway operations. It is generated by vibrations of both the rail and the wheel that are excited at their interface. In general rail vibration is more complex than wheel vibration since the track is effectively infinite and contains components with pronounced non-linear behaviour. Many different models have been developed to investigate the dynamic properties of railway track over the years. These models can be divided into four main groups: (a) an infinite, uniform beam continuously supported by damped resilient and mass layers (railpads, sleepers and ballast) [1–4]; (b) periodically supported uniform Euler or Timoshenko beams [1, 2, 5, 6]; (c) finite element meshed rail supported by continuous pads, sleepers and ballast foundation [7, 8]; (d) finite element meshed

† On leave from the Department of Mechanical Engineering, Shanghai Tiedao University, Shanghai 200331, The People's Republic of China.

0022–460X/99/050881 + 24 $30.00/0

rail cross-section model with periodic supports [9]. Models (a) and (b) are usually considered to have a good agreement with measurements in the frequency region where the cross-sectional deformation of rail does not appear. The predictions obtained by using models (a) and (b) are better for rail vertical vibration than for lateral vibration, for example, the periodically supported Timoshenko beam model may be used for vertical vibration up to about 1500 Hz. Models (c) and (d) are more useful for predicting high frequency rail vibration and for both vertical and lateral vibrations because the rail cross-sectional deformation is included in them. The need to include periodic supports, models (b) and (d), is greater for tracks with stiff railpads and is generally more important for the vertical direction than the lateral direction.

In all these models the resilient components in the foundation layers or at the periodic supports such as the railpad and the ballast have significant effects on the track vibration, noise radiation, the contact force between rail and wheel and the generation of rail corrugations. Usually, their parameters are considered uniform in these models. For example, the pad stiffness and the ballast stiffness are regarded as constant along the whole railway track or assigned the same value at each support. In fact these parameters vary with load and frequency. Measurements [10, 11] have shown that the pad stiffness can vary dramatically with preload and also varies with vibration frequency. The ballast stiffness is also strongly dependent upon load and frequency [12]. When a train moves along the rail, it applies a preload on the rail and its foundation in a local area around each wheel. Therefore, the pad stiffness and the ballast stiffness near the wheel are different from those which apply at a distance along the rail. This affects the dynamic behaviour of the track, thus the rail vibration, noise radiation, contact force etc. Obviously these parameter variations with wheel preload should be taken into consideration in these models especially for the vertical vibration.

The aim of this paper is to study the vertical rail vibration properties considering the pad and ballast stiffness variations due to wheel preload. Although the behaviour of pads and ballast is non-linear, it is assumed that the dynamic behaviour can be represented by a linear model with stiffnesses that are chosen according to the quasi-static load, since the dynamic displacements are small. Firstly the non-linear load–deflection and load–stiffness laws for both railpad and ballast are introduced according to [10] and [12]. Then they are combined to obtain the load–deflection property of the whole rail foundation. After this, the rail deflection and the reaction force in the foundation under a wheel load are calculated in order to obtain the different preloads in the pad and ballast at the different supports along the track. Knowing the preloads in the pad and ballast, the dynamic stiffness of the preloaded pad and ballast can be determined from data in references [10] and [12]. Finally a discretely supported Timoshenko beam model is employed and the receptances and the wave propagation decay rates for vertical rail vibration are calculated considering the preloaded pad and ballast stiffnesses which have different values at different supports. The method derived here is applied to a track consisting of UIC 60 rails on monobloc concrete sleepers. The railpads are Pandrol studded 10 mm pads. This study shows that when the preloaded pad and ballast stiffness are considered, the results are quite different

from the model in which only the uniform values of the pad and ballast stiffness are employed. However, it is possible to derive an approximate method for using the simpler model by a combination of loaded and unloaded parameter values.

2. STIFFNESS OF RAILWAY TRACK FOUNDATION

In order to determine the preloaded pad and ballast stiffnesses, the values of preload in the pad and ballast should be known in advance. In practice this preload is caused by the weight of trains and is transmitted through the wheels to the rail and its foundation. It is effectively a static problem to determine the preload in the pad and ballast. Only one wheel load is considered for simplicity and at this stage the railway track is simplified to an infinite uniform beam on a continuous elastic foundation. However, this foundation, composed of railpads and ballast, has a non-linear behaviour because both railpad and ballast stiffnesses are non-linear. Therefore, the non-linearity of the railway track foundation should be studied first.

2.1. PAD STIFFNESS

Both the static and dynamic stiffness of the railpad considered here have been measured by Thompson *et al*. [10]. The static load-deflection and load-stiffness curves are shown in Figure 1, the stiffness being defined here as the inverse of the gradient of the load–deflection curve. The static stiffness can be seen to be relatively constant for preloads up to 25 kN, above which it increases sharply. Values of the static and dynamic stiffness at selected preloads are given in Table 1. The dynamic stiffness is mildly frequency dependent and the values given in Table 1 apply at the frequencies listed. It can be seen that the dynamic stiffness is much higher than the static stiffness at the same preload level. The dynamic/static stiffness ratio is used in sections 4 and 5. In general, the rail is fixed to the sleepers by clips. The clip applies a preload on the railpad which is about 20 kN for each pad. In addition the weight of the rail is also applied onto the pad as a preload. For UIC 60 rail (60 kg/m) and a 0·6 m distance between two sleepers

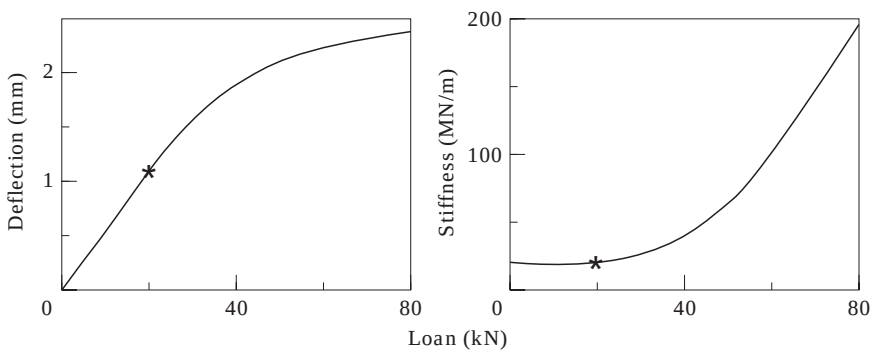

Figure 1. Static load–deflection and load–stiffness curves for Pandrol studded 10 mm railpad (redrawn from [12]). *initial preload point.

TABLE 1

Static and dynamic stiffness of Pandrol studded 10 mm *railpad* (*from* [10])

Preload (kN)	20	30	40	60	80
Static stiffness (MN/m)	19	25	37	95	200
Dynamic stiffness at 50 Hz (MN/m)	61	82	130	300	650
Dynamic stiffness at 200 Hz (MN/m)	69	92	140	330	690
Dynamic stiffness at 500 Hz (MN/m)	81	110	170	390	780
Dynamic/static stiffness ratio at 50 Hz	3·2	3·3	3·5	3·2	3·3
Dynamic/static stiffness ratio at 200 Hz	3·6	3·7	3·8	3·5	3·6
Dynamic/static stiffness ratio at 500 Hz	4·3	4·4	4·6	4·1	3·9

each railpad is subjected to about 0·36 kN rail weight load. Thus the initial preload in the railpad is about 20·36 kN. In Figure 1 this preload point is marked by '*'.

2.2. BALLAST STIFFNESS

Detailed data for the ballast stiffness are not available at present, but some work on the ballast stiffness is helpful to estimate the elastic properties of the railway foundation. According to direct dynamic measurements, some points about the ballast stiffness variation have been highlighted by Frémion *et al*. [12]. It is found that vertical stiffness of the ballast is influenced by a static preload and increases significantly with the frequency. They suggested that the ballast stiffness may be assumed to follow the Hertz law because the law in $W^{1/3}$ is consistent with the experimental results, where W is the static preload. A summary of the direct stiffness measurements from [12] is given in Table 2. It can be seen that a doubling of the ballast stiffness occurs from 50 Hz to 200 Hz and again from 200 Hz to 500 Hz, and changing the preload from 1·2 kN to 11 kN leads to a doubling of the vertical stiffness. However, when the preload increases from 11 to 21 kN, the vertical stiffness increases only by about 15%.

By use of the data in Table 2 and the suggestion that the vertical stiffness follows the Hertz law, one assumes that the ballast stiffness k_b can be represented by

$$k_b = a\sqrt[3]{f_b}, \tag{1}$$

where f_b and a are the load and the constant coefficient respectively. Because stiffness is the derivative of the load with respect to the deflection u; $k_b = \mathrm{d}f_b/\mathrm{d}u$, the load–deflection law for ballast can be derived from it and has the form of

$$u = (1{\cdot}5/a)\sqrt[3]{f_b^2}. \tag{2}$$

TABLE 2

Vertical ballast stiffness for a sleeper block with an area of 0·23m^2 (*from* [12])

Static load (kN)	50 Hz (MN/m)	200 Hz (MN/m)	500 Hz (MN/m)
1·2	50	130	–
11	120	210	420
21	125	240	480

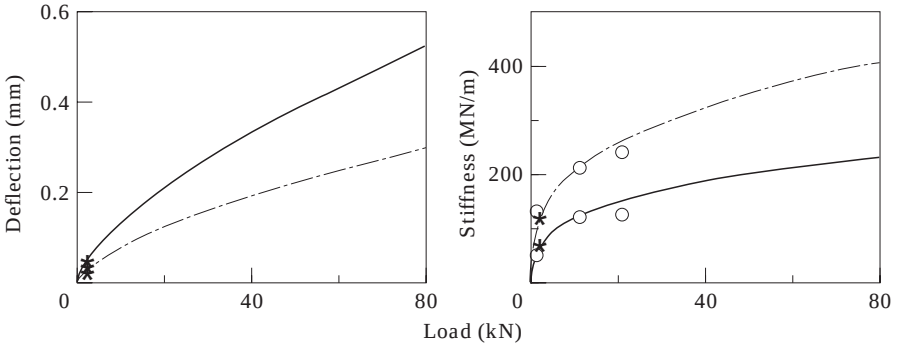

Figure 2. Dynamic load-deflection and load-stiffness curves for ballast at 50 Hz and 200 Hz. — at 50 Hz; – · –, at 200 Hz; *, initial preload point; o, points from Table 2.

The load–stiffness and load–deflection curves for the ballast at 50 Hz and 200 Hz are shown in Figure 2, where the constant coefficient a is determined using the data at the static load 11 kN. The ballast stiffness can be seen to increase very sharply when preload increases from zero and the rate of increase of the ballast stiffness becomes smaller as the preload increases further. Therefore, the increment tendency of the ballast stiffness is the opposite of that of the pad stiffness. The initial preload in the ballast is from the rail weight and the sleeper weight. A monobloc concrete sleeper weighs about 3 kN. The weight of half a sleeper and 0·6 m rail forms the initial preload in the ballast at each support, which is about 1·86 kN and marked by '*' in Figure 2. Some other data about the ballast stiffness can be found in Appendix A, which confirm the load–deflection relationship given above.

2.3. RAILWAY TRACK FOUNDATION STIFFNESS

The elasticity of the rail foundation is formed by both railpad and ballast, but now the superposition principle does not hold because of their non-linearity. To obtain the load–deflection and load–stiffness laws of the foundation the whole evolution of the deformation from zero in the pad and ballast should be taken into consideration. Figure 3 shows the loads on the pad and the ballast. W_r and W_s represent the weights of the rail in one span and of the sleeper respectively. f_c is the preloads from the clips. f is the external load and Δu_p and Δu_b represent deflections of the pad and the ballast respectively caused by f. The following values are used for the parameters (as above): $W_r = 0{\cdot}36$ kN, $W_s = 1{\cdot}5$ kN, $f_c = 20$ kN.

The foundation deflection u should be equal to the sum of the pad deflection and the ballast deflection:

$$u = \Delta u_p + \Delta u_b. \tag{3}$$

Since the clip stiffness is much softer than the pad, f_c can be regarded as constant when the pad is subjected to a deformation caused by the external load f. Thus

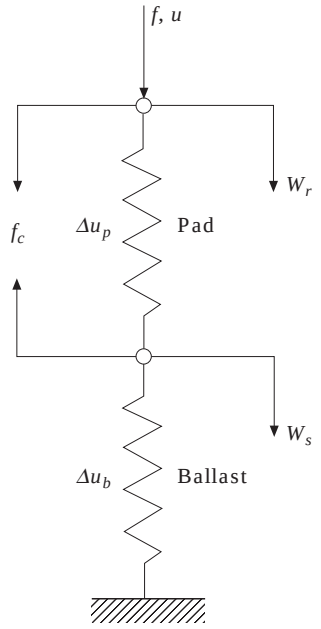

Figure 3. Loads on the pad and ballast.

the pad deflection Δu_p and the ballast deformation Δu_b under the external load f can be written as

$$\Delta u_p = u_p(f + f_c + W_r) - u_p(f_c + W_r), \qquad \Delta u_b = u_b(f + W_r + W_s) - u_b(W_r + W_s), \tag{4a, b}$$

where $u_p(f)$ and $u_b(f)$ are the deflections as a function of load of the pad and ballast respectively.

Because the data for the ballast static stiffness are not available, it is assumed here that the ballast static stiffness may be estimated to have values that are 25, 50 or 100% of the dynamic stiffness at 50 Hz, which are represented as soft, medium and stiff ballast respectively. Using the load–deflection curves in Figure 1 for the pad and the load–deflection law in equation (2) for the ballast, the

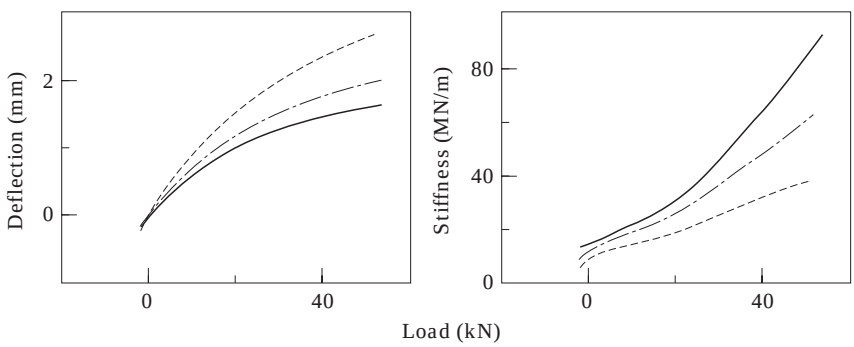

Figure 4. Foundation load-deflection and load-stiffness curves. —, stiff ballast; – · –, medium ballast; - - -, soft ballast.

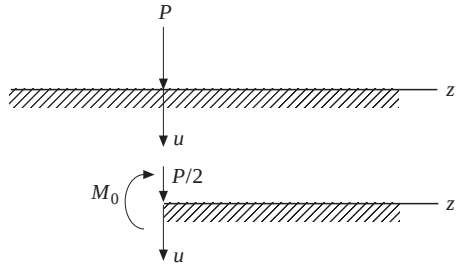

Figure 5. Beam on the elastic foundation. By symmetry with suitable boundary conditions the upper system can be replaced by the lower system.

load–deflection law for the complete rail foundation can be obtained by equations (3) and (4). Figure 4 shows these combined load–deflection and load–stiffness curves of the rail foundation. The load–stiffness curve is derived from the load–deflection curve. Three graphs are shown, respectively, the soft, medium and stiff ballast assumptions. It can be seen that the rail foundation retains non-linearity.

3. DEFLECTION AND REACTION FORCE IN THE RAILWAY FOUNDATION UNDER THE WHEEL LOAD

3.1. EQUATION FOR THE BEAM ON A NON-LINEAR ELASTIC FOUNDATION

In order to determine the deflection and reaction force in the track foundation due to a wheel load, the wheel load can be represented by a concentrated load and the railway track is simplified to an infinite uniform beam supported by a continuous elastic foundation. For the beam on a linear elastic foundation Timoshenko gave an exact solution in reference [13]. However, the railway track foundation considered here is non-linear rather than having a constant modulus. This makes the problem much more difficult to solve than the linear elastic case.

The differential equation for the rail deflection has the form of

$$EI\,\mathrm{d}^4u/\mathrm{d}z^4 = -f(u)/d, \tag{5}$$

where $f(u)$ is the reaction force in the foundation of one span as a function of deflection u and d is the span length. EI is the bending stiffness of the beam and z is the distance along the track. $f(u)$ is determined by the load–deflection law in Figure 4. The rail and sleeper weights vanish now because their effect has already been included in the procedure of deriving the load–deflection law of the foundation. Only half of the beam need be considered due to the symmetry condition at the load point, see Figure 5. The boundary conditions for equation (5) are:

$$u'(0) = 0, \qquad u'''(0) = P/2EI, \qquad u(\infty) = 0, \qquad u'(\infty) = 0, \qquad \text{(6a–d)}$$

where P is the wheel load acting at the position $z = 0$ and $'$ indicates the derivative with respect to z. Boundary conditions (6c) and (6d) mean that at points infinitely distant from the load P the deflection and the slope vanish.

3.2. NUMERICAL SOLUTIONS—DEFLECTION AND REACTION FORCE IN FOUNDATION

Equation (5) with the boundary conditions (6) forms a non-linear boundary value problem which may be solved numerically. It is difficult to solve because equation (5) is a fourth order differential equation and some boundary conditions in (6) should be satisfied at the infinitely distant points. The starting point for the numerical calculation should be chosen at $z = 0$. There are two parameters at $z = 0$ which have to be estimated in order to meet the boundary conditions at $z = \infty$. These are $u(0)$ and $u''(0)$. For performing the numerical calculation some points should be considered:

(1) It is impossible to meet the boundary conditions at $z = \infty$ because the errors introduced by numerical approximations will ruin the solution as z becomes very large. By referring to the analytical solution of the beam on a linear elastic foundation, a reasonable value may be estimated for z, at which the boundary conditions should be satisfied instead of at $z = \infty$. In the case of the linear elastic foundation the beam deflection is given as in [13]:

$$u = (P\beta/2k)\, \mathrm{e}^{-\beta z}(\cos \beta z + \sin \beta z) \tag{7}$$

where $\beta = \sqrt[4]{k/(4EI)}$, k is the constant modulus of the foundation. The deflection can be seen to decay very quickly with the power of $-\beta z$. u', u'' and u''' have the same decay rate as u. From the authors' experience, the boundary conditions at $z = \infty$ may be regarded as the boundary conditions at $z = 4 \sim 5$ m.

(2) Since there are two values required at the beginning, $u(0)$ and $u''(0)$, the normal "shooting method" [14] is not appropriate. Here a simple direct 2-D searching method is developed. It is divided into two stages. Firstly, the searching procedure is performed in a larger area with a large step size to obtain a rough solution. Then the same procedure is performed but in a small area and with a fine step size. This method is found to be quite effective for 2-D searching.

The numerical results of both the foundation deflection and the reaction force in the foundation are shown in Figure 6, where the span length $d = 0{\cdot}6$ m, the wheel load $P = 75$ kN and $EI = 6{\cdot}4 \times 10^6$ Nm^2 for UIC 60 rail. Three curves are shown representing the results from the soft, medium and stiff ballast stiffness assumptions. It can be seen that the foundation deformation occurs only in the near field of the wheel load. At $z = 0$, where the load P acts, the deflection has its maximum value, but from about $z = 2{\cdot}3$ m for the stiff ballast, $z = 2{\cdot}5$ m for the medium one and $z = 3$ m for the soft one the foundation deflection is almost zero (Note—although negative deflection occurs, neither the ballast nor the pad unload completely). The stiffer the foundation, the smaller the maximum deflection at $z = 0$, and the quicker the decay of the deflection. The decay rate of the deflection is similar to that in the case of the linear elastic foundation, in which it is $\mathrm{e}^{-\beta z}$. The curve of the reaction force in the foundation is similar to the deflection. The reaction force also occurs only in the near field of the wheel load and has the maximum value at $z = 0$. The stiffer foundation has a larger maximum reaction force. For the reaction force the decay rate is also higher for the stiffer foundation, but in the area near to $z = 0$ it is noticeably sharper than the deflection decay. This is because the stiffness of the foundation increases with increasing

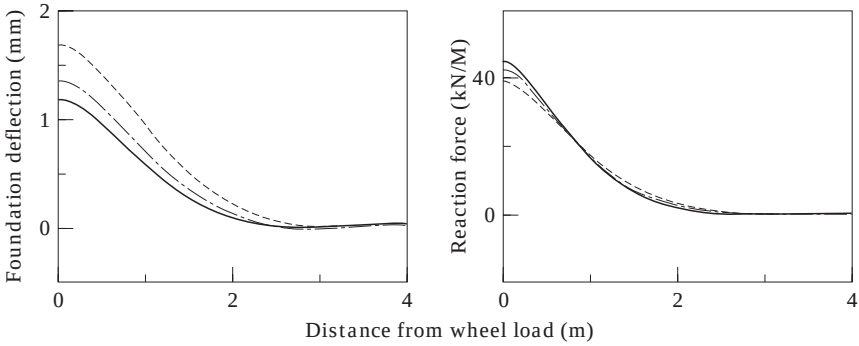

Figure 6. Foundation deflection and reaction force under 75 kN wheel load. Key as for Figure 4.

deflection. For smaller deflections the foundation is softer, and thus the reaction force is smaller.

For comparison, Figure 7 shows the foundation deflection and the reaction force from a linear elastic foundation model having a constant modulus k equivalent to the medium ballast assumption and the wheel load $P = 75$ kN. k is chosen to give the same maximum deflection as the non-linear elastic foundation,

$$u(0) = P\beta/2k, \tag{8}$$

where $u(0)$ is the deflection at $z = 0$ from the non-linear foundation model, and $\beta = \sqrt[4]{k/(4EI)}$. It can be seen from Figure 7 that the foundation deflection of the linear model is quite close to that of the non-linear model, but the reaction force is not as sharp as in the non-linear model. The region with negative deflection and reaction force is greater in the linear case than in the non-linear case. It should be pointed out that there is no general approximate linear solution for the non-linear elastic foundation model because the equivalent constant stiffness needs to be determined using the deflection at $z = 0$ from the non-linear model.

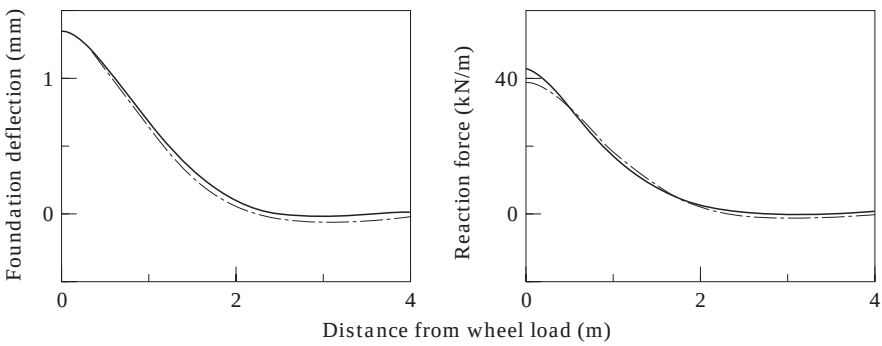

Figure 7. Comparison of the results from non-linear foundation model and equivalent linear foundation model, $P = 75$ kN, medium ballast. —, non-linear foundation; – · –, linear foundation ($k = 28{\cdot}71$ MN/m^2).

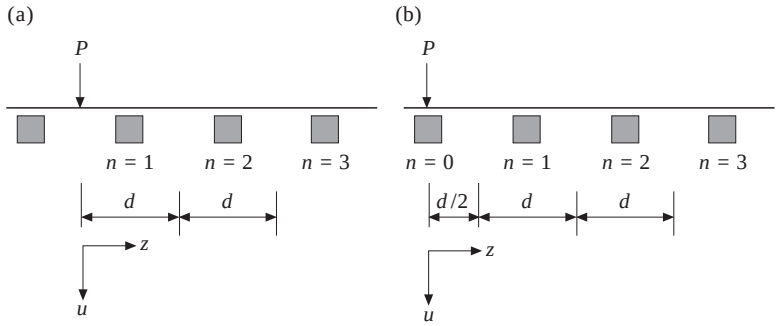

Figure 8. Integral limits for calculating the preload at each support. (a) load at mid-span, (b) load above a sleeper.

4. PAD AND BALLAST STIFFNESSES UNDER PRELOAD

4.1. PRELOAD IN PAD AND BALLAST

The pad and ballast stiffnesses are dependent on the preload in them. Under the wheel load, the foundation deflection and reaction force have different values at different places so that the railpads and ballast are subjected to different preloads at different supports. The preloads in the pad and ballast can be calculated on the basis of the foundation deflection $u(z)$ and the load–deflection law $f[u(z)]$ as derived in the previous sections. Two situations are considered here to determine the preloads in the pad and the ballast. In the first the wheel load is acting at mid-span (half way between two sleepers), and in the other the wheel load is acting above a sleeper.

The preload P_f in the foundation at different supports can be obtained by performing the following definite integral between corresponding limits z_1 and z_2:

$$P_f = \int_{z_1}^{z_2} \frac{f[u(z)]}{d}\,\mathrm{d}z. \tag{9}$$

Figure 8 shows schematically the integral limits for calculating the preload at each support in the two wheel load situations. For the wheel load acting at mid-span, the integral limits are from $(n-1)d$ to nd for the nth support. For the wheel load acting above a sleeper the integral limits are from 0 to $d/2$ for the first support ($n = 0$) and the integral should be doubled. For the others the integral limits are from $(2n-1)d/2$ to $(2n+1)d/2$ for the nth support.

The results of the preloads in pad and ballast at different supports are listed in Tables 3 and 4 for the wheel loads $P = 75$ and 125 kN respectively. The same parameters as in the previous sections are used. The preload in the pad P_p includes the clip load f_c and the rail weight. The preload in the ballast P_b includes the rail and sleeper weights. They are calculated by using following equations:

$$P_p = P_f + f_c = W_r, \qquad P_b = P_j + W_r + W_s. \tag{10a, b}$$

It can be seen from Tables 3 and 4 that the preloads in the pad and ballast reach the maximum values at the nearest support to the wheel load, and decrease with

increasing the distance from the wheel load. The effects of the wheel load on the preloads in the pad and ballast are seen only at a limited number of supports, for example, five supports at each side of the wheel load. Except for these supports, the preload at other supports further away from the wheel load may be approximately regarded as only having rail weight and clip loads for the pad, rail and sleeper weight loads for the ballast. Therefore, the influence of the wheel loads on the preloads in the pad and ballast is local. Compared with the wheel loads acting at mid-span, when the wheel load acts above a sleeper, the pad and the ballast at that support will bear a larger preload. The changing of the ballast stiffness from soft to stiff only causes a slight difference in the preloads of the pad and ballast. When the ballast stiffness changes from soft to stiff, the preload distribution at different supports becomes slightly more localised in the vicinity of the wheel.

4.2. PRELOADED PAD AND BALLAST STIFFNESS

The preloaded pad and ballast stiffnesses can be determined from their load-stiffness laws. In reference [10] it is found that the pad dynamic stiffness varies slightly with frequency. At 200 Hz the dynamic stiffness to static stiffness ratio is about from 3·5–3·8 and this can be used to derive a load-dependent but frequency-independent approximation (see Table 1). For higher frequency it is slightly higher than this. Here a ratio of 3·6 is used for the pad dynamic stiffness.

TABLE 3

Preloads (kN) *in pad and ballast caused by a wheel load of* 75 kN

Wheel load / Static ballast stiffness		Above a sleeper ($P = 75$ kN)			At a midspan ($P = 75$ kN)		
		Soft	Medium	Stiff	Soft	Medium	Stiff
Pad position	0	43·84	45·66	46·88	–	–	–
	1	36·86	37·28	37·47	41·54	42·86	43·71
	2	28·46	27·94	27·54	32·34	32·13	31·90
	3	23·28	22·67	22·33	25·45	24·81	24·40
	4	20·96	20·54	20·41	21·84	21·31	21·08
	5	20·30	20·08	20·13	20·50	20·18	20·14
	6	–	–	–	20·27	20·12	20·26
	∞	20·36	20·36	20·36	20·36	20·36	20·36
Ballast position	0	25·34	27·16	28·38	–	–	–
	1	18·36	18·78	18·97	23·04	24·36	25·21
	2	9·96	9·44	9·38	13·84	13·63	13·40
	3	4·78	4·17	3·83	6·95	6·31	5·90
	4	2·46	2·04	1·91	3·34	2·81	2·58
	5	1·80	1·58	1·63	2·00	1·68	1·64
	6	–	–	–	1·77	1·62	1·76
	∞	1·86	1·86	1·86	1·86	1·86	1·86

TABLE 4

Preloads (kN) *in pad and ballast caused by a wheel load of* 125 kN

Wheel load / Static ballast stiffness		Above a sleeper ($P = 125$ kN)			At a midspan ($P = 125$ kN)		
		Soft	Medium	Stiff	Soft	Medium	Stiff
Pad position	0	63·01	67·52	71·14	–	–	–
	1	48·20	48·39	48·07	58·07	60·92	62·89
	2	32·51	31·21	30·26	39·32	38·25	37·27
	3	24·36	23·36	22·79	27·67	26·46	25·67
	4	21·02	20·48	20·29	22·25	21·48	21·13
	5	20·16	19·96	20·03	20·40	20·04	19·99
	6	–	–	–	20·14	20·07	20·24
	∞	20·36	20·36	20·36	20·36	20·36	20·36
Ballast position	0	44·51	49·02	52·64	–	–	–
	1	29·70	29·89	29·57	39·57	42·42	44·39
	2	14·01	12·71	11·76	20·82	19·75	18·77
	3	5·86	4·86	4·29	9·17	7·96	7·17
	4	2·52	1·98	1·79	3·75	2·98	2·63
	5	1·66	1·46	1·53	1·90	1·54	1·49
	6	–	–	–	1·64	1·57	1·74
	∞	1·86	1·86	1·86	1·86	1·86	1·86

The ballast stiffness is also frequency dependent, but less data are available. In order to allow for the larger area of ballast in contact with a monobloc sleeper, the ballast stiffness at 200 Hz in Table 2, which was measured with bibloc sleepers, has been multiplied by 1·3 for calculating the ballast dynamic stiffness. Note that the soft, medium and stiff approximations apply only to the static ballast stiffness and not the dynamic stiffness, which is the same in each case.

The preloaded pad and ballast dynamic stiffnesses in different wheel load situations are listed in Tables 5 and 6. The stiffness variation is similar to the preload variation in Tables 3 and 4. At the nearest support to the wheel load the pad and ballast stiffnesses have the maximum values, and gradually reduce to some stable value with increasing distance from the wheel load. These stable values are the stiffness of the pad under the clip load and the rail weight and the stiffness of the ballast under the rail and sleeper weights. The effects of the wheel load on the pad and ballast stiffness are also local, for example, on five pads and the ballast under five sleepers at each side of the wheel load. For other pads and sleepers more distant from the wheel load, their stiffness may approximately be regarded as uniform. Comparing the data in Table 5 to those in Table 6 one can see that the stiffness of the preloaded pads at the supports near the wheel load dramatically increases when the wheel load increases from 75 to 125 kN. This is because the pad stiffness increases sharply if the preload is above 40 kN (see Figure 1). The ballast stiffness also increases when the wheel load goes up, but not so sharply.

5. VERTICAL RAIL VIBRATION CONSIDERING PRELOADED PAD AND BALLAST STIFFNESS

5.1. DISCRETELY SUPPORTED RAILWAY TRACK MODEL

The dynamic railway track model used for exploring the vertical vibration behaviour under the local wheel load is shown in Figure 9. It is represented by an infinite uniform Timoshenko beam which is discretely supported by the railpads, sleepers and ballast. The beam is characterised by EI, the bending stiffness, G, the shear modulus, ρ, the density, A, the cross-sectional area, κ, the shear coefficient and η_r, the damping loss factor. The nth railpad is modelled by a stiffness K_{pn} and a damping loss factor η_p. The subscript n indicates that the pad stiffness may have different values at different supports because the pads are subjected to the preloads due to the local deformation of the track foundation caused by the train weight. The pad loss factor is assumed constant, consistent with measurements in [10]. The sleeper is modelled as a mass M_s. The ballast is modelled by a stiffness K_{bn} and a damping loss factor η_b. The subscript n again indicates that the ballast stiffness may have different values at different supports due to the preload. Since the train speed is much lower than the flexural wave propagation speed in the rail, the dynamic excitation imposed by the rolling wheel is represented by a stationary harmonic force $F\,e^{i\omega t}$, where $i = \sqrt{-1}$ and ω is the angular frequency of the harmonic excitation.

TABLE 5

Preloaded pad and ballast dynamic stiffness (MN/m) *for wheel load* 75 kN

Wheel load / Static ballast stiffness		Above a sleeper ($P = 75$ kN)			At a midspan ($P = 75$ kN)		
		Soft	Medium	Stiff	Soft	Medium	Stiff
Pad position	0	161·4	174·4	183·7	–	–	–
	1	119·7	121·9	122·9	146·7	155·1	160·5
	2	86·9	85·3	84·1	99·6	98·9	98·1
	3	73·2	72·3	71·8	78·0	76·1	74·9
	4	69·8	69·1	68·8	71·0	70·2	69·9
	5	68·7	68·3	68·4	69·0	68·5	68·4
	6	–	–	–	68·6	68·4	68·6
	∞	68·8	68·8	68·8	68·8	68·8	68·8
Ballast position	0	360·6	369·0	374·5	–	–	–
	1	323·9	326·3	327·4	349·3	355·9	360·0
	2	264·1	259·4	255·7	294·8	293·2	291·6
	3	206·8	197·5	192·1	234·2	226·9	221·9
	4	165·8	155·8	152·3	183·4	173·3	168·3
	5	149·3	142·9	144·6	154·6	146·0	144·9
	6	–	–	–	148·4	144·2	148·2
	∞	151·0	151·0	151·0	151·0	151·0	151·0

TABLE 6

Preloaded pad and ballast dynamic stiffness (MN/m) *for wheel load* 125 kN

Static ballast stiffness	Wheel load	Above a sleeper ($P = 125$ kN)			At a midspan ($P = 125$ kN)		
		Soft	Medium	Stiff	Soft	Medium	Stiff
Pad position	0	376·3	473·7	551·1	–	–	–
	1	193·6	195·0	192·6	330·2	357·5	375·2
	2	100·2	95·7	92·6	132·8	127·1	121·9
	3	74·8	73·3	72·4	84·5	81·0	78·6
	4	69·8	69·0	68·7	71·6	70·5	69·9
	5	68·5	68·2	68·3	68·8	68·3	68·2
	6	–	–	–	68·4	68·3	68·6
	∞	68·8	68·8	68·8	68·8	68·8	68·8
Ballast position	0	435·1	449·3	460·1	–	–	–
	1	380·2	381·0	379·6	418·3	428·1	434·7
	2	296·0	286·5	279·2	337·7	331·8	326·3
	3	221·3	207·9	199·5	256·9	245·1	236·7
	4	167·1	154·1	149·1	190·7	176·7	169·4
	5	145·3	139·2	141·5	152·0	141·9	140·3
	6	–	–	–	144·8	142·6	147·7
	∞	151·0	151·0	151·0	151·0	151·0	151·0

The discretely supported track model can be treated in various ways. One approach is developed by Heckl [15]. In this approach the discrete rail supports are replaced by corresponding external forces, and thus the railway track can be simply considered as an infinite beam with many point forces acting on it. Based on the Green's function and the superposition principle the stationary response of the rail to the harmonic excitation can be obtained. In addition although the beam is infinite, it is modelled with a finite number of supports, this number being chosen large enough to guarantee a reliable approximate solution. This approach is also employed here but now the support stiffness is not uniform due to the wheel load. Moreover the symmetry of the railway track about the forcing point for

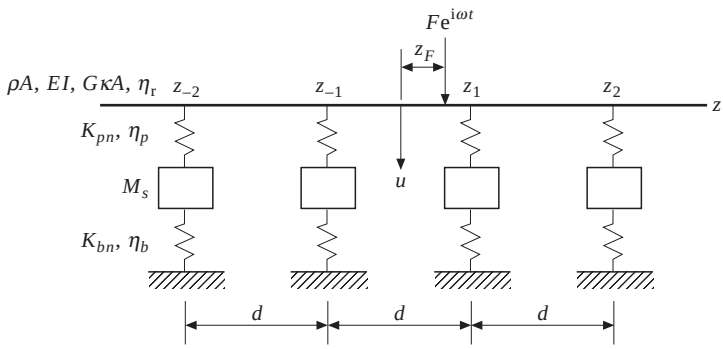

Figure 9. Discretely supported railway track model.

excitation above a sleeper or at mid-span is taken into account to increase the efficiency of the calculation.

The Green's function $G(z, z')$ for an infinite Timoshenko beam is the response at point z to a unit harmonic force at z' [16]:

$$G(z, z') = (u_1 \, e^{-ik_1|z - z'|} + u_2 \, e^{-k_2|z - z'|}) \, e^{i\omega t}, \tag{11}$$

where k_1 and k_2 are the respective complex wavenumbers of the propagating and evanescent waves in the free Timoshenko beam, given by

$$k_1 = (\omega/\sqrt{2})\{\rho/E + \rho/G\kappa + [(\rho/E - \rho/G\kappa)^2 + 4\rho A/EI\omega^2]^{1/2}\}^{1/2}, \tag{12a}$$

$$k_2 = (\omega/\sqrt{2})\{-(\rho/E + \rho/G\kappa) + [(\rho/E - \rho/G\kappa)^2 + 4\rho A/EI\omega^2]^{1/2}\}^{1/2}, \tag{12b}$$

and u_1 and u_2 are defined by

$$u_1 = \frac{i}{EG\kappa} \frac{\rho I\omega^2 - G\kappa A - EIk_1^2}{2Ak_1(k_1^2 + k_2^2)}, \qquad u_2 = \frac{1}{EG\kappa} \frac{\rho I\omega^2 - G\kappa A - EIk_2^2}{2Ak_2(k_1^2 + k_2^2)}. \tag{13a, b}$$

Here the formulation given in [15] has been modified by the inclusion of the shear coefficient κ and more convenient notation as in [16]. The rail loss factor is included in these equations by making E and G complex with the factor $(1 + i\eta_r)$.

Consider now such a beam attached to the supports with dynamic stiffness Z_n at the position $z = z_n$, see Figure 9. A single external harmonic force $F \, e^{i\omega t}$ acts at the point $z = z_F$. The dynamic stiffness Z_n is the ratio of force to the displacement caused by that force and given by

$$Z_n = \frac{K_{pn}(1 + i\eta_p)[K_{bn}(1 + i\eta_b) - M_s\omega^2]}{K_{pn}(1 + i\eta_p) + K_{bn}(1 + i\eta_b) - M_s\omega^2}. \tag{14}$$

The total displacement u at a point z is given by the superposition of the response to the external force $F \, e^{i\omega t}$ and the response to the forces from all the support points:

$$u(z) = -\sum_{\substack{n = -N \\ n \neq 0}}^{N} Z_n u(z_n) G(z, z_n) + FG(z, z_F). \tag{15}$$

The displacement at each support point $z = z_m$ can be given by

$$u(z_m) = -\sum_{\substack{n = -N \\ n \neq 0}}^{N} Z_n u(z_n) G(z_m, z_n) + FG(z_m, z_F), \qquad m = \pm 1, \pm 2, \ldots, \pm N \tag{16}$$

From equation (16) the displacements at each support point can be solved in terms of F by taking the sum to the left side and then inverting the matrix of coefficients of $u(z_m)$. Substituting them into equation (15), one can obtain the displacement at any point on the rail.

If the external force $F \, e^{i\omega t}$ acts at mid-span or above a sleeper, the symmetry of the problem can be used to reduce the dimension of equations (15) and (16). For example, when $F \, e^{i\omega t}$ acts at mid-span where $z = 0$ and thus $z_F = 0$, the

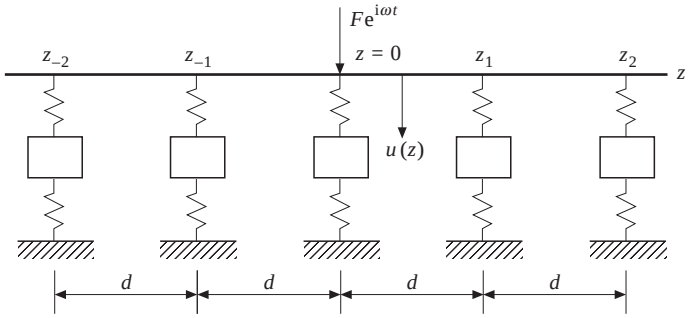

Figure 10. Special case of discretely supported track model where external force acts above a sleeper.

displacements are symmetric with respect to the point $z = 0$ and the following relationship holds:

$$u(z) = u(-z), \qquad Z_n = Z_{-n}, \qquad G(z, z') = G(-z, -z'). \tag{17a–c}$$

Thus only half the support point displacements in equations (15) and (16) need to be determined. Equations (15) and (16) can now be simplified by using equation (17) to give

$$u(z) = -\sum_{n=1}^{N} Z_n u(z_n)[G(z, z_n) + G(z, -z_n)] + FG(z, 0), \tag{18}$$

$$u(z_m) = -\sum_{n=1}^{N} Z_n u(z_n)[G(z_m, z_n) + G(z_m, -z_n)] + FG(z_m, 0),$$

$$m = 1, 2, \ldots N. \tag{19}$$

For the external force acting above a sleeper, again taking the forcing point as $z = 0$ (see Figure 10), the displacements can be determined by the following equations considering the symmetric conditions:

$$u(z) = -Z_0 u(0)G(z, 0) - \sum_{n=1}^{N} Z_n u(z_n)[G(z, z_n) + G(z, -z_n)] + FG(z, 0), \tag{20}$$

$$u(z_m) = -Z_0 u(0)G(z, 0) - \sum_{n=1}^{N} Z_n u(z_n)[G(z_m, z_n) + G(z_m, -z_n)] + FG(z, 0),$$

$$m = 0, 1, 2, \ldots, N. \tag{21}$$

By using symmetric conditions the computing time is reduced dramatically because only half the number of displacements need to be calculated.

5.2. NUMERICAL RESULTS

The point receptance of the track for vertical vibration is calculated for the external excitation acting either above a sleeper or at mid-span in the frequency

range from 50–1500 Hz. The wave propagation decay rate along the rail is examined in the same frequency range. To investigate the effects of the local wheel load on the track vertical vibration behaviour the preloaded pad and ballast stiffnesses listed in Tables 5 and 6 are employed in the numerical calculation and the results are compared to those from the track model having uniform pad and ballast stiffnesses. The following parameters are used in numerical calculations: $E = 2 \times 10^{11}$ N/m^2, $G = 0{\cdot}77 \times 10^{11}$ N/m^2, $\eta_r = 0{\cdot}01$, $\rho = 8000$ kg/m^3, $A = 0{\cdot}75 \times 10^{-2}$ m^2, $I = 3{\cdot}2 \times 10^{-5}$ m^4, $\kappa = 0{\cdot}4$, $M_s = 150$ kg, $\eta_p = 0{\cdot}25$, $\eta_b = 0{\cdot}6$, $d = 0{\cdot}6$ m, $N = 40$ (for receptance), $N = 60$ (for decay rate). These are chosen to represent UIC 60 rail [17] and the sleeper mass represents half of the mass of a concrete monobloc sleeper. The ballast loss factor is chosen lower than in [17] in order to make effects in the response more visible.

Because the deformation of the track foundation caused by the wheel load is local and only a limited number of pads and ballast springs are preloaded by the wheel load, the pad and ballast stiffnesses are assigned different values at only the first six supports on each side of the wheel load (including $n = 0$ for the case of excitation above a sleeper) and from the seventh support they have uniform values. The preloaded pad and ballast stiffnesses listed in Tables 5 and 6 for the stiff ballast assumption are used in the calculation.

5.2.1. *Receptance*

The amplitude and phase of the point receptances of the track are shown in Figures 11 and 12 which give the results for the wheel load $P = 75$ and 125 kN respectively. Figures 11(a) and 12(a) show the results when the wheel load acts at

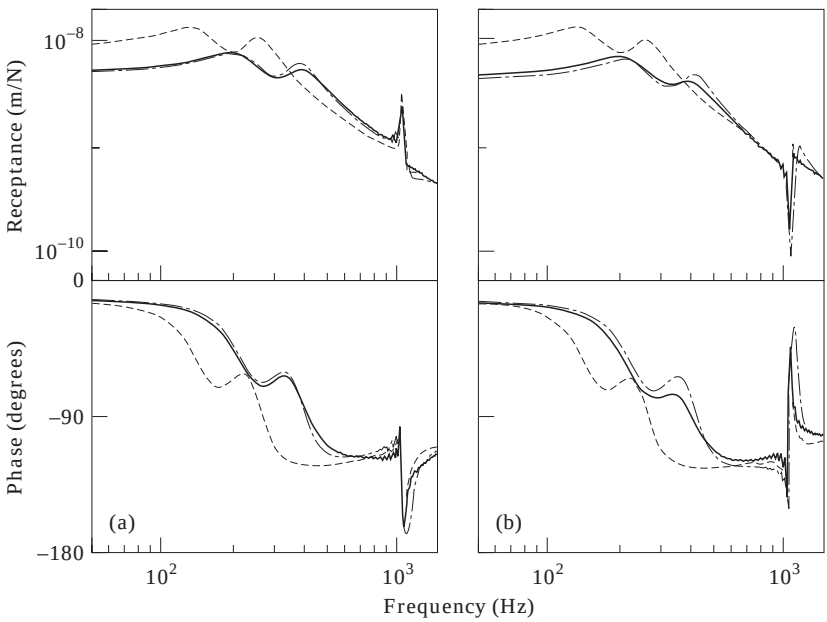

Figure 11. Amplitude and phase of the point receptances, for $P = 75$ kN. (a) load at mid-span, (b) load above a sleeper. —, varying stiffness foundation; – · –, uniform stiff foundation; - - -, uniform soft foundation.

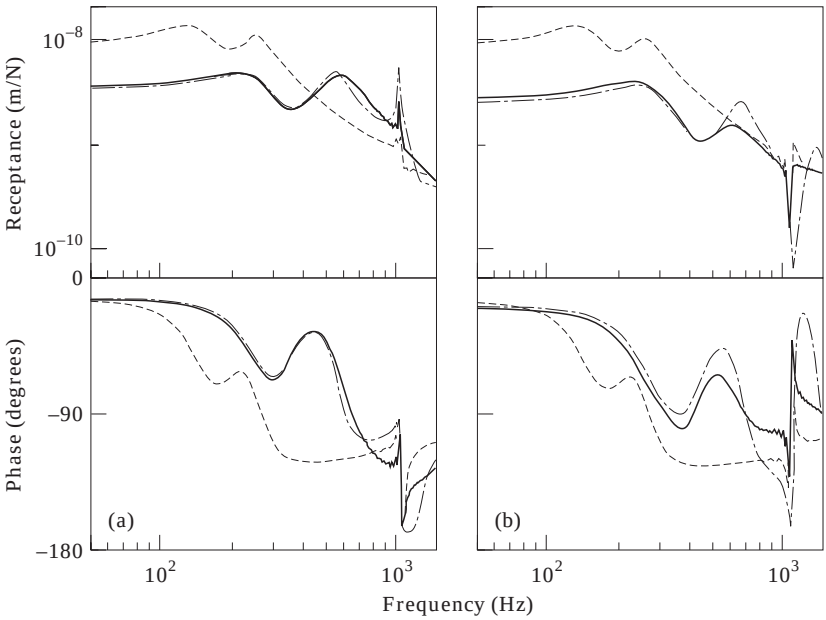

Figure 12. Amplitude and phase of the point receptances, for $P = 125$ kN. (a) load at mid-span, (b) load above a sleeper. Key as for Figure 11.

mid-span and Figures 11(b) and 12(b) show the results when the wheel load acts above a sleeper. The solid lines in Figures 11 and 12 are the results from the model having different pad and ballast stiffness at different supports near the wheel load. The dotted lines are the results from the model having uniform pad and ballast stiffness at each support point which has the values as at the seventh support point—this case represents a uniform soft or unloaded foundation. The dotted–dashed lines also are the results from the model having uniform pad and ballast stiffness but which has the values as at the first support point—this case represents the uniform stiff or loaded foundation.

Two well-damped resonances can be seen, at about 130 and 260 Hz for the uniform soft foundation model. These occur at higher frequencies for both the uniform stiff foundation and the varying stiffness foundation models—in Figure 11 where $P = 75$ kN they occur at about 200 and 400 Hz and in Figure 12 where $P = 125$ kN they occur at about 220 and 600 Hz. At the first resonance the whole track bounces on the ballast stiffness, whereas at the second the rail vibrates on the pad stiffness. At about 1050 Hz the pinned–pinned resonance, which corresponds to a standing wave with nodes at the sleepers, can be seen for all the models although there are different peak values from different models.

It can be seen from Figures 11 and 12 that the uniform stiff foundation model and the varying stiffness foundation model have almost the same receptance curves in the frequency range up to about 1000 Hz. Based on this it may be considered that *the point receptances of a railway track at low frequencies* (*below the pinned–pinned resonance*) *are governed by the local supports near the wheel load*. This point can be further verified by the curves in Figure 13. The solid lines in Figure 13 come from the rail on the uniform stiff foundation under the wheel load

$P = 75$ kN, and the dotted lines come from the same rail but having only three uniform supports for the wheel load acting above a sleeper ($n = 0, \pm 1$), or four uniform supports for the wheel load acting at mid-span ($n = \pm 1, \pm 2$). The fact that these two lines almost overlap each other except near the pinned–pinned frequency indicates again that the receptances of a railway track at low frequencies are controlled by only a few supports near the wheel load. In addition it can be seen from Figures 11 and 12 that the stiffer the foundation, the lower the receptances in the low frequency region and the higher the frequencies corresponding to the two low frequency resonances of the rail vibration.

With regard to the pinned–pinned resonance peaks, it can be seen from Figures 11 and 12 that the peak is higher in the case of the uniform stiff foundation than the uniform soft or varying stiffness foundations, whereas in the latter two cases the peaks are equally high. The first fact implies that the pinned–pinned resonance is stronger when the rail foundation is stiffer and the second implies that *the local stiffness variation in the rail foundation near the wheel load has no obvious effects on the pinned–pinned resonance*.

5.2.2. *Decay rate*

The decay rates of the wave propagation along the rail for different models are shown in Figures 14 and 15. These are calculated from the decay in vibration level over a thirty span length from the excitation point divided by this distance (18 m). The curves in Figure 14 are for the wheel load $P = 75$ kN and in Figure 15 for $P = 125$ kN. Figures 14(a) and 15(a) show the results when the wheel load acts at mid-span and Figures 14(b) and 15(b) show the results when the wheel load acts

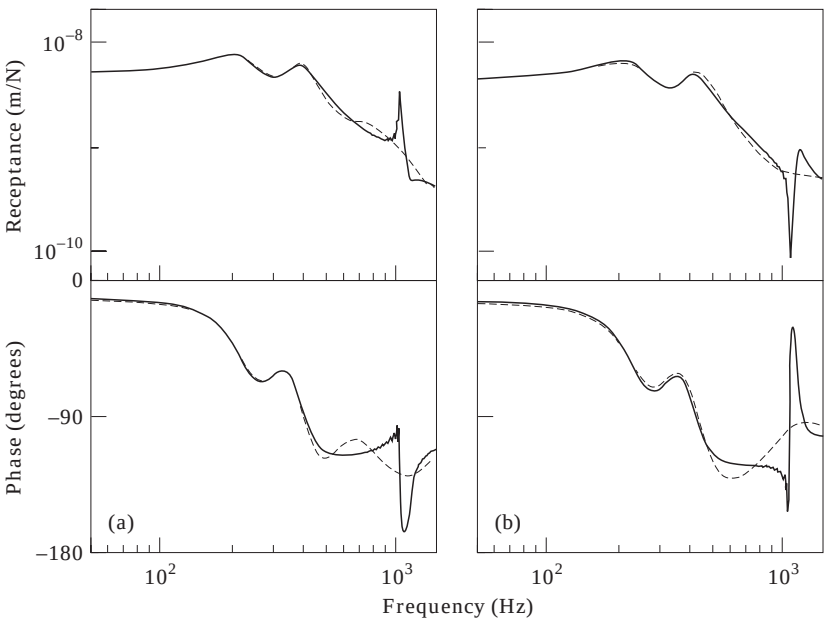

Figure 13. Amplitude and phase of the point receptances, for $P = 75$ kN. (a) load at mid-span, (b) load above a sleeper. —, uniform stiff foundation; - - -, four uniform supports for load at mid-span and three uniform supports for load above a sleeper.

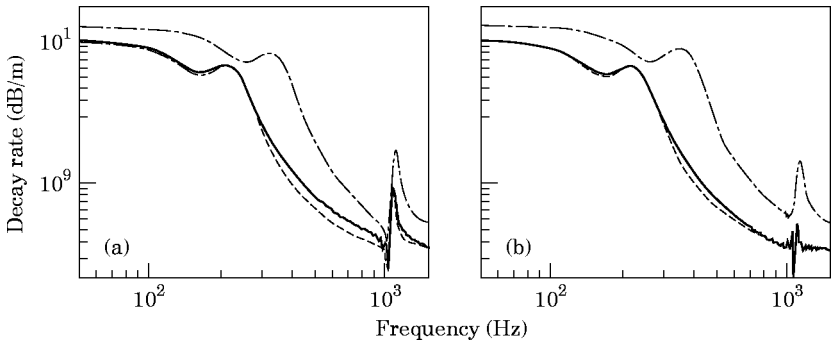

Figure 14. Decay rates of the wave propagation along the rail, for $P = 75$ kN. (a) load at mid-span, (b) load above a sleeper. Key as for Figure 11.

above a sleeper. The solid lines here again represent the varying stiffness foundation model. The dotted lines represent the uniform soft foundation model and the dotted–dashed lines represent the uniform stiff foundation model. In general for all models, the decay rates can be seen to be very high in the low frequency region and very low in the high frequency region. They gradually decrease with increasing frequency and then reach a local trough and a local peak. For the uniform foundation models this peak corresponds to a trough in the receptance. After the peak the decay rates drop steeply, and then have a sharp peak just above the pinned–pinned resonance frequency. It can be seen from Figures 14 and 15 that the decay rate is higher in the case of the uniform stiff foundation than the uniform soft and varying stiffness foundations, whereas in the latter foundations the decay rates are almost the same for both values of the wheel load $P = 75$ or 125 kN. This implies that *the effect of the local stiffness variation in the track foundation near the wheel load on the average wave propagation decay rate is very limited*. The reason for this is that the pad and ballast are stiffened only at a few supports near the wheel load and therefore their effects on the average decay rate within a certain distance are not very noticeable. However, within about two or three spans from the wheel load the local decay rate is higher than in distant area due to the local loaded and thus stiffer supports. As an example Figure 16

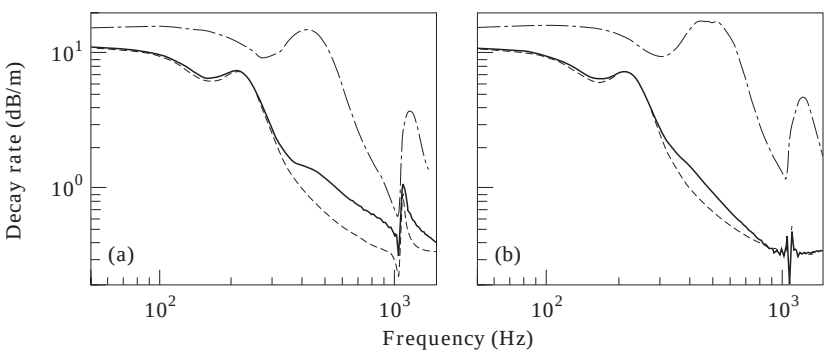

Figure 15. Decay rates of the wave propagation along the rail, for $P = 125$ kN. (a) load at mid-span, (b) load above a sleeper. Key as for Figure 11.

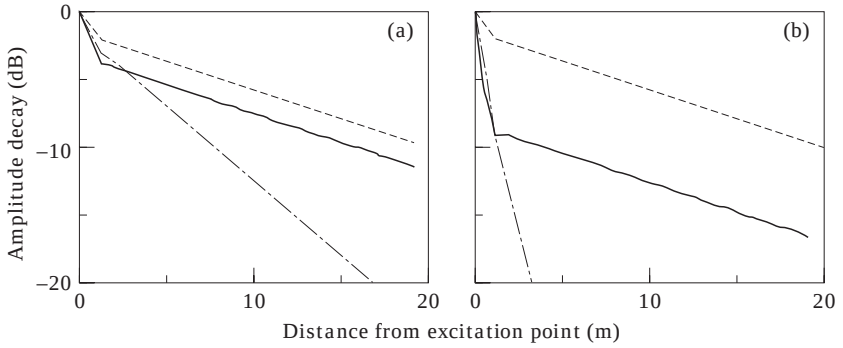

Figure 16. Amplitude of the transfer receptance at 600 Hz, load at mid-span. (a) for $P = 75$ kN, (b) for $P = 125$ kN. Key as for Figure 11.

shows the amplitude decay of the transfer receptance which represents the response at other positions along the rail to a unit harmonic force acting at $z = 0$. In this case the exciting frequency is 600 Hz. The solid lines in Figure 16 represent the varying stiffness foundation model, the dotted lines the uniform soft foundation model and the dotted–dashed lines the uniform stiff foundation model. Figure 16(a) is for the wheel load $P = 75$ kN and Figure 16(b) for the wheel load $P = 125$ kN. The amplitude decay rate can be seen to be higher only in a local area near the excitation point for the varying stiffness foundation model and to be almost equal far from the excitation point for both varying stiffness foundation and uniform soft foundation. This example at 600 Hz corresponds to a region in Figures 14 and 15 where the varying stiffness and uniform soft foundation results differed most.

Based on the facts that the point receptances at low frequencies are governed by the local supports near the wheel load, whereas the pinned–pinned resonance and the average decay rate of the wave propagation are determined by the unloaded supports, a simpler vertical track vibration model may be a combination of a few (three or four) preloaded supports near the external excitation and unloaded supports at the other points along the rail. It would also be possible to approximate the vertical track vibration using a combination of a model with loaded supports to represent the receptance and a model with unloaded supports to represent the average decay rate. Nevertheless, such an approximation would overestimate the receptance at the rail-on-pad resonance, here between 400 and 600 Hz, by up to 4·5 dB.

6. CONCLUSION

In this paper the effects of a single wheel preload on the railway foundation stiffness and vertical vibration have been studied. Firstly the non-linear load–deflection relationship of the whole track foundation was obtained by combining the pad and ballast load–deflection laws. Based on this load–deflection law of the track foundation, the local foundation deformation caused by a single static wheel load was obtained using a non-linear track model and hence the

preloads in the pad and ballast are known. From a knowledge of the load–frequency–stiffness laws of the pad and ballast, their dynamic stiffness at different supports around the wheel load can be determined. To investigate the effect of the preloaded pad and ballast stiffness on the track vertical vibration an infinite discretely supported Timoshenko beam model has been employed, and the point receptance of the rail and the wave propagation decay rate were calculated by using different track foundation models including the uniform soft, uniform stiff and varying stiffness foundations.

The results show that the deformations of the track foundation under a single static wheel load are local and near the wheel load, so only a limited number of railpads and ballast springs are preloaded by the wheel load. The preloaded pads and ballast become stiffer and thus affect the railway vertical vibration behaviour to some extent. The numerical predictions show that the track vertical vibration properties below the pinned–pinned resonance frequency are noticeably influenced through the stiffened pad and ballast due to the static wheel preload. The receptance of the rail vibration is reduced at low frequency and the first two resonance frequencies are increased when the preloaded pad and ballast stiffnesses are employed in the vertical track vibration model. A good approximation to the receptance is given by using the loaded stiffness throughout. On the other hand, the local static wheel load does not affect the pinned–pinned resonance and affects the average wave propagation decay rate along the rail only to a very limited extent, and these can be predicted from the uniform unloaded (soft support) track model.

This paper has given a general approach to investigate the influence of the local preload on track vertical vibration and useful results have been obtained. Further practical measurements need to be carried out to validate the predictions and also essentially, more detailed information about the ballast static and dynamic stiffness is needed.

REFERENCES

1. S. L. Grassie, R. W. Gregory, D. Harrison and K. L. Johnson 1982 *Journal Mechanical Engineering Science* **24**, 77–90. The dynamic response of railway track to high frequency vertical excitation.
2. D. J. Thompson and N. Vincent 1995 *Vehicle System Dynamics* Supplement **24**, 86–99. Track dynamic behaviour at high frequencies. Part 1: theoretical models and laboratory measurements.
3. Y. Sato 1977 *JNR*, *Railway Technical Reviews*, *Quarterly Reports* **18**, 109–114. Study on high frequency vibrations in track operated with high-speed trains.
4. D. G. Duffy 1990 *Journal of Applied Mechanics* **57**, 66–73. The response of an infinite railroad track to a moving, vibrating mass.
5. B. Ripke and K. Knothe 1991 *Fortschritt-Berichte VDI* Reihe 11, Nr. 155. Die unendlich lange Schiene auf diskreten Schwellen bei harmonischer Einzellasterregung. (The infinitely long rail on discrete sleepers with harmonic point force excitation).
6. M. A. Heckl 1992 *Proceedings of DAGA* 92, 1033–1036. Anregung von gekoppelten Wellen auf einem Timoshenko-Balken mit äquidistanten Stutzstellen (Generation of coupled waves in a Timoshenko beam with equidistant supports).

7. D. J. THOMPSON 1993 *Journal of Sound and Vibration* **161**, 421–446. Wheel–rail noise generation, part III: rail vibration.
8. D. J. THOMPSON 1990 *Ph.D. Thesis*, *University of Southampton*. Wheel–rail noise: theoretical modelling of the generation of vibrations.
9. L. GRY 1996 *Journal of Sound and Vibration* **195**, 477–505. Dynamic modelling of railway track based on wave propagation.
10. D. J. THOMPSON, W. J. VAN VLIET and J. W. VERHEIJ 1998 *Journal of Sound and Vibration* **213**, 169–188. Developments of the indirect method for measuring the high frequency dynamic stiffness of resilient elements.
11. Å. FENANDER 1997 *Proceedings of the Institution of Mechanical Engineers Part F* **211**, 51–62. Frequency dependent stiffness and damping of railpads.
12. N. FRÉMION, J. P. GOUDARD and N. VINCENT 1996 *VIBRATEC Report* 072.028*a*. Improvement of ballast and sleeper description in TWINS—step 1: experimental characterisation of ballast properties.
13. S. TIMOSHENKO 1958 *Strength of Materials*, *Part II Advanced Theory and Problems*. New Jersey: D. Van Nostrand; third edition.
14. R. L. BURDEN and J. D. FAIRES 1993 *Numerical Analysis*. Boston: International Thompson; fifth edition.
15. M. A. HECKL 1995 *Acustica* **81**, 559–564. Railway noise—can random sleeper spacing help?
16. D. J. THOMPSON and M. H. A. JANSSENS 1994 *TNO report TPD-HAG-RPT*-93-0214. TWINS: Track-wheel interaction noise software. Theoretical manual, version 2.2.
17. N. VINCENT and D. J. THOMPSON 1995 *Vehicle System Dynamics* Supplement **24**, 100–114. Track dynamic behaviour at high frequencies. Part 2: experimental results and comparisons with theory.
18. A. IGELAND and J. OSCARSSON 1996 *Report F*193, Division of Solid Mechanics, Chalmers University of Technology. Modelling of railway track for computer simulation of dynamic train/track interaction.

APPENDIX A: APPROXIMATIONS TO STATIC BALLAST STIFFNESS MEASURED BY IGELAND AND OSCARSSON

In the model presented in the current paper, it has been assumed that the relationship between the reaction force, f and the displacement, u of ballast has the form:

$$f = bu^{3/2}. \tag{A1}$$

This has been based on very small amount of measurement points from reference [12]. In reference [18] Igeland and Oscarsson give the results of more comprehensive measurements of the static stiffness of ballast, performed at a site known as Goose Hill in Sweden. The monobloc concrete sleepers were disconnected from the rail and a load was applied to both the railseats of one sleeper. The deflection of the sleeper end was measured against a fixed datum. The results are reproduced in Figure A1(a) in which the load given is applied at each railseat. Surprisingly large differences in the sleeper end deflection were found between adjacent sleepers.

Before comparing these results with those from reference [12], it should be noted that the latter results are based on a single block with base size 0·84 m × 0·28 m. In the results from reference [18] the sleeper is three times longer (2·5 m) so that the overall stiffness can be expected to be greater. What is of interest here,

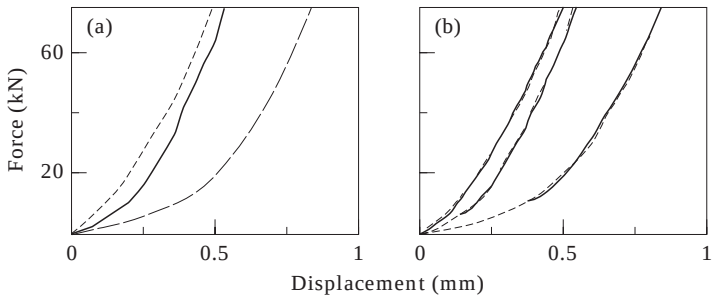

Figure A1. Load applied to concrete monobloc sleeper at each rail seat versus deflection at sleeper end. (a) Measured from [18]; —, sleeper 2; — —, sleeper 4; - - - , sleeper 5. (b) ——, approximations based on equation (A2), - - - , measurements from (a).

however, is whether an expression of the form assumed in equation (A1) is also appropriate to the data from reference [18]. Fitting an expression of this form to the results from reference [18] gives a good fit for sleeper S5, but a poor fit for the other sleepers. Sleepers S2 and S4 appear to be more closely represented by a higher power, u^2 and $u^{5/2}$ respectively.

However, it may be noted that sleepers S2 and S4 exhibit a significant initial deflection for only a small load, following which the results for all three sleepers appear to have a similar slope. This suggests that a more appropriate model may be one of the form:

$$f = f_0 + b(u - u_0)^{3/2} \quad \text{for} \quad u > u_0. \tag{A2}$$

Results for such a model are given in Figure A1(b). They can be seen to be a good approximation to the measured results for appropriate choice of u_0 and f_0. The slope parameter b, is found to be in the range $6{\cdot}4 \times 10^9$–$8{\cdot}3 \times 10^9\ \mathrm{Nm}^{-3/2}$ for all three sleepers. This means that the variations found between the stiffnesses of the adjacent sleepers are likely to be due not to the material behaviour of the ballast or ground, but to the initial "slack" in the ballast under each sleeper. These values of b correspond roughly to the 50 Hz dynamic stiffness values given in Table 2.

The measured data from reference [18] therefore appear to give reasonable support to the use of a stiffness law such as equation (A1). Significant variations are found, not in the stiffness law itself, but in the initial part of the load–deflection curve.